Nanoscale Fullerene Compression of an Yttrium Carbide Cluster

Jianyuan Zhang,[†] Tim Fuhrer,[†] Wujun Fu,[†] Jiechao Ge,[†] Daniel W. Bearden,[‡] Jerry Dallas,[‡] James Duchamp,[†] Kenneth Walker,[§] Hunter Champion,[†] Hugo Azurmendi,[†] Kim Harich,[†] and Harry C. Dorn*[,†,‖]

[†]Department of Chemistry, Virginia Polytechnic Institute and State University, Blacksburg, Virginia 24060, United States
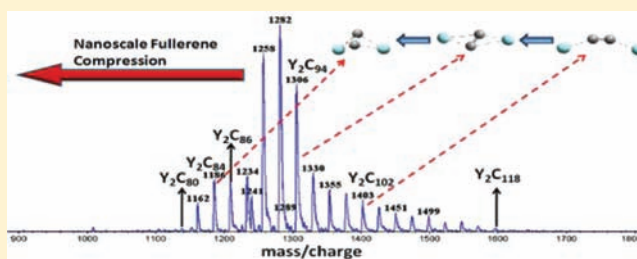
[‡]National Institute of Standards and Technology, Analytical Chemistry Division, Hollings Marine Laboratory, Charleston, South Carolina 29412, United States

[§]Luna Innovations, Inc. (nanoWorks Division), 521 Bridge Street, Danville, Virginia 24541, United States

[‖]Virginia Tech Carilion Research Institute, Roanoke, Virginia 24016, United States

S Supporting Information

ABSTRACT: The nanoscale parameters of metal clusters and lattices have a crucial influence on the macroscopic properties of materials. Herein, we provide a detailed study on the size and shape of isolated yttrium carbide clusters in different fullerene cages. A family of diyttrium endohedral metal-lofullerenes with the general formula of Y_2C_{2n} (n = 40−59) are reported. The high field ^{13}C nuclear magnetic resonance (NMR) and density functional theory (DFT) methods are employed to examine this yttrium carbide cluster in certain family members, $Y_2C_2@D_5(450)$-C_{100}, $Y_2C_2@D_3(85)$-C_{92},

$Y_2C_2@C_{84}$, $Y_2C_2@C_{3v}(8)$-C_{82}, and $Y_2C_2@C_s(6)$-C_{82}. The results of this study suggest that decreasing the size of a fullerene cage with the same $(Y_2C_2)^{4+}$ cluster results in nanoscale fullerene compression (NFC) from a nearly linear stretched geometry to a constrained "butterfly" structure. The ^{13}C NMR chemical shift and scalar $^1J_{YC}$ coupling parameters provide a very sensitive measure of this NFC effect for the $(Y_2C_2)^{4+}$ cluster. The crystal structural parameters of a previously reported metal carbide, Y_2C_3 are directly compared to the $(Y_2C_2)^{4+}$ cluster in the current metallofullerene study.

INTRODUCTION

Isolation of metal clusters from adjacent lattice units frees them from their usual intramolecular interactions, and provides a paradigm of understanding their size and shape within constrained models. A recent seminal example of this approach is the encapsulation of a single water molecule in the fullerene C_{60} which isolates it from other water molecules preventing intramolecular hydrogen bonding.[1] For metal clusters, fullerene carbon cages also provide ideal environments for the isolation purpose to study the size and shape of metal lattice and other important structural nanoscale parameters thereby tuning their physical properties.

Our hypothesis is that decreasing the fullerene cage size of endohedral metallofullerenes (EMFs) will dramatically change the size and shape of the encapsulated metal clusters. Furthermore, nanoscale fullerene compression (NFC) of the metal clusters by decreasing fullerene cage size can be directly compared with macroscopic pressure compression (MPC) of the same metal carbide lattice of yttrium carbides. Herein, we present a detailed structural investigation of the yttrium carbide clusters in progressing from large ($\sim C_{100}$) to smaller fullerene cages (C_{82}). The results learned from the isolated model can be related to the metal lattice in other systems, for example, in superconducting metal carbide systems.[4] We also compare

crystal structural parameters of a previously reported metal carbide, Y_2C_3 to the $(Y_2C_2)^{4+}$ cluster in the current metal-lofullerene study illustrating the influence of nanoscale FC when compared with the effects of macroscopic external pressure compression.[2,3] In the Y_2C_3 superconducting system, the superconducting transition temperature (T_c) of Y_2C_3 is strongly dependent on the external pressure.[4]

To date, the metal clusters encapsulated in the fullerene cages have included: metal atoms,[5−9] metal clusters,[10−14] metal nitride clusters[15,16] and metal carbide clusters.[17−25] The encapsulated metal carbide clusters reported to date have fullerene cages ranging from C_{68} to C_{92} but the attempts to detect the ^{13}C chemical shifts of the endohedral carbide cluster were not successful until Nagase et al. utilized isotopically enriched ^{13}C samples.[23] Single crystal structures of $Gd_2C_2@$ C_{92}[22] and two $Sc_2C_2@C_{82}$ isomers[26,27] have been studied, and a very recent X-ray crystal study of $Sc_2C_2@C_{2n}$ (n = 40−42) shows the change in carbon cage size can result in different carbide cluster shapes.[25] For a clear understanding of the structural changes of the metal carbide clusters as a function of cage size, we have performed a detailed ^{13}C NMR study of the

yttrium−carbide dimetallofullerenes, $Y_2C_2@D_3$-C_{92}, ^{13}C enriched $Y_2C_2@C_{3v}$-C_{82}, and $Y_2C_2@C_s$-C_{82}[18] as well as an isomer of $Y_2C_2@C_{84}$. For the first time, we have observed the important scalar $^1J_{Y−C}$ coupling for all samples. In addition, the experimental results are supported by DFT calculations of the $(Y_2C_2)^{4+}$ cluster in various environments, including the cluster $(Y_2C_2)^{4+}$, $Y_2C_2@D_5$-C_{100}, $Y_2C_2@D_3$-C_{92}, and $Y_2C_2@C_{3v}$-C_{82}.

A previous DFT computational study of the Y_2C_2 neutral molecular cluster supports a stable linear structural arrangement as illustrated (Figure 1a), although a square planar
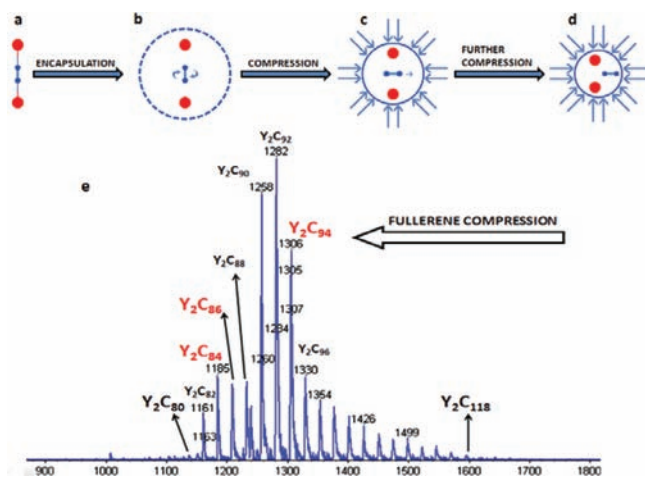

Figure 1. Nanoscale fullerene compression of yttrium carbide clusters. (a) $Y_2C_2^{4+}$ cluster without a cage; (b) linear $Y_2C_2^{4+}$ cluster inside a large fullerene cage; (c) $Y_2C_2^{4+}$ cluster with carbide bond vector orthogonal to the yttrium−yttrium vector in a compressed fullerene cage; (d) $Y_2C_2^{4+}$ cluster with carbide bond vector orthogonal to and deviated from yttrium−yttrium vector; (e) mass spectrometry showing a family of endohedral metallofullerenes with formula Y_2C_{2n}.

structure is only slightly less stable.[28] For the charged $(Y_2C_2)^{4+}$ cluster, the DFT results of our current study also suggest a stable linear structure stable linear structure (Figure 1b). However, the study on metallofullerenes encapsulating other metals (Gd and Sc) also established that the $(M_2C_2)^{4+}$ metal-carbide clusters inside mid-sized fullerene cages can have the carbide bond vector orthogonal to the metal−metal bond adopting an "idealized butterfly shape" (as in $Gd_2C_2@C_{92}$, Figure 1c).[22] An additional increase in the compression of the $(M_2C_2)^{4+}$ cluster by a small cage leads to a butterfly shape in which the carbide is orthogonal to but displaced from the metal−metal bond axis (as in $Sc_2C_2@C_{82}$, Figure 1d).[26] We propose that this structural difference is due to the cage size rather than the metal, and a certain encapsulated $(M_2C_2)^{4+}$ cluster in a progressively smaller cage changes the most stable cluster conformation from a linear to butterfly shape.

The endohedral metallofullerene (EMF) synthesis was accomplished by arcing the Y_2O_3 filled graphite rods in helium. A family of EMFs with the formula Y_2C_{2n} ($n = 40−59$) was obtained that dominated the mass spectrum after selective removal of empty caged fullerenes (Figure 1e).[29] Although some of the peaks in Figure 1e could result from classic dimetallic EMFs $Y_2@C_{2n}$, we have isolated four yttrium carbide members of this family, $Y_2C_2@C_{3v}$-C_{82}, $Y_2C_2@C_s$-C_{82}, $Y_2C_2@C_{84}$ and the larger cage $Y_2C_2@D_3$-C_{92} for our experimental study.

EXPERIMENTAL SECTION

Synthesis and Isolation of $Y_2C_2@D_3$-C_{92}. $Y_2C_2@D_3$-C_{92} was synthesized in a Krätschmer-Huffman generator by vaporizing composite graphite carbon rods filled with a mixture of Y_2O_3, graphite powder, and metallic Cu with a weight ratio of 1.1/1.0/2.1 in a dynamic flow of He and N_2 (flow rate ratio of N_2/He = 3/100). The produced soot was then extracted with refluxing toluene in a Soxhlet extractor and soluble extract was applied to a cyclopentadiene-functionalized Merrifield peptide resin column. The eluent from the column was separated by multistage HPLC. The purity of $Y_2C_2@C_{92}$ was confirmed by HPLC chromatogram, laser-desorption time-of-light
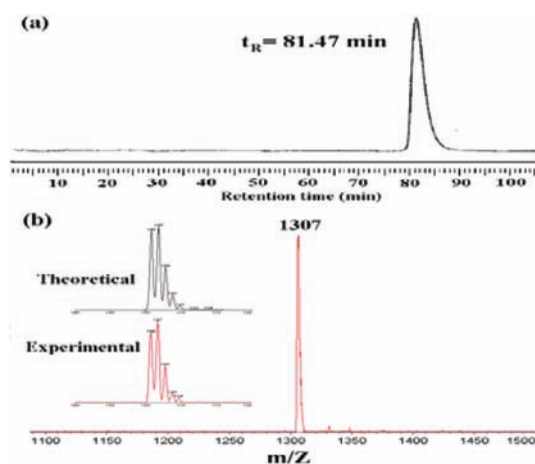

Figure 2. (a) HPLC chromatography of $Y_2C_2@D_3$-C_{92} (a 10 × 250 mm 5PYE column; λ = 390 nm; flow rate 2.0 mL/min; toluene as eluent; 25 °C); (b) LD-TOF mass spectrum of $Y_2C_2@D_3$-C_{92} with positive ionization.

(LD-TOF MS) mass spectrometry (Figure 2) and UV−vis spectral characterization (Supporting Information Figure S1) and cyclic voltammetry (Supporting Information Figure S6) were also performed. A Raman spectroscopic study of this sample describing tunneling of the carbide has been reported.[30]

Synthesis and Isolation of $Y_2C_2@C_{3v}$-C_{82}, $Y_2C_2@C_s$-C_{82}, and $Y_2C_2@C_{84}$. The ^{13}C labeled yttrium carbide EMFs were produced in a similar process with Krätschmer-Huffman generator, with one graphite electrode filled with Y_2O_3 and ^{13}C labeled amorphous carbon powder (99% Cambridge Isotopes). The mass ratio between ^{13}C packed amorphous carbon powder and the graphite rod wall was 1/3. After solvent extraction, the soluble portion of the soot was applied to a modified "stir and filter approach" with cyclopentadiene-functionalized silica (instead of amino-functionalized silica) to remove the majority of the empty-cage fullerenes while maintaining a significant portion of the yttrium carbide EMFs.[29] The resulting solution was loaded onto a 5-PBB column for chromatographic separation. The $Y_2C_2@C_s$-C_{82} and $Y_2C_2@C_{3v}$-C_{82} were co-eluted with the $Y_3N@C_{80}$, and the $Y_2C_2@C_{84}$ was co-eluted with $Y_3N@C_{82}$. With further multistage isolation on a 5-PYE HPLC column, the $Y_2C_2@C_{3v}$-C_{82}, $Y_2C_2@C_s$-C_{82}, and $Y_2C_2@C_{84}$ were obtained and the corresponding chromatograms of the purified products are shown in Figure 3a,c,e. These EMFs are also characterized by LD-TOF mass-spectrometry (Figure 3b,d,f) and UV−vis spectrum (see Supporting Information). To ensure the accuracy of the molecular mass of the ^{13}C enriched peaks in the mass spectra, the well-characterized EMF $Sc_3N@C_{80}$ (m/z = 1109) was used as an internal mass calibrator in $Y_2C_2@C_s$-C_{82}, as shown in Figure 3d. The molecular peak in the mass spectrum is broadened and shifted to higher mass by 7−8 mass units (1193 rather than 1186 for Y_2C_{84} and 1218 instead of 1210 for Y_2C_{86}), suggesting a ~9% ^{13}C enrichment.

^{13}C NMR Sample Preparation and Spectroscopy. EMF samples were dissolved in 90% CS_2/10% CD_3COCD_3 and
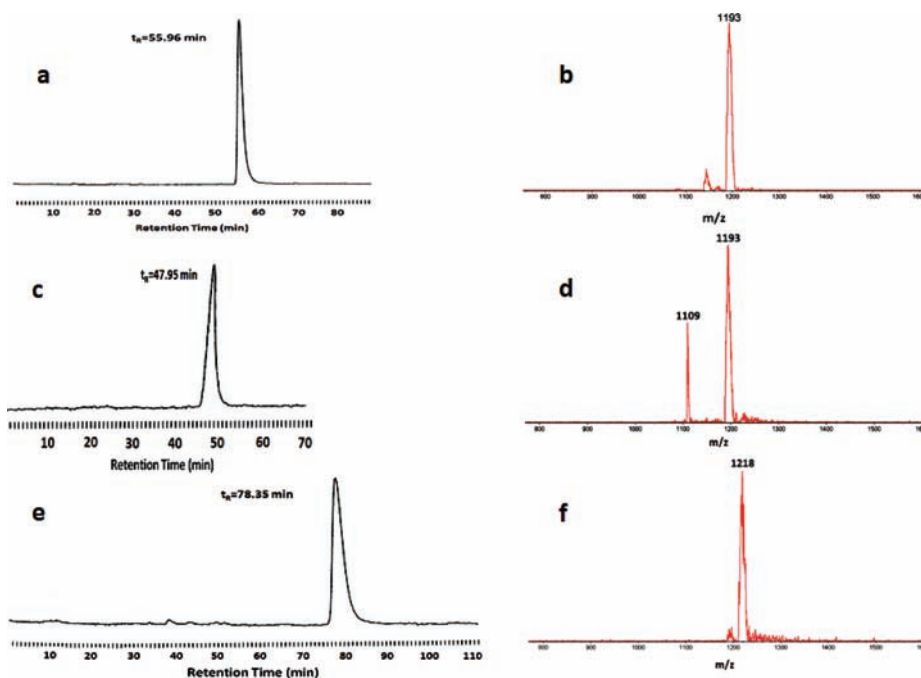
Figure 3. (a) HPLC chromatogram of $Y_2C_2@C_{3v}$-C_{82} (a 10 × 250 mm 5PYE column; λ = 390 nm; flow rate 2.0 mL/min; toluene as eluent; 25 °C). (b) LD-TOF mass spectra of ^{13}C enriched $Y_2C_2@C_{3v}$-C_{82} with positive ionization. The two smaller peaks are M-24 and M-48, respectively, resulted from the loss of C_2 units in the ionization process. (c) HPLC chromatogram of $Y_2C_2@C_s$-C_{82}. (d) LD-TOF mass spectra of ^{13}C enriched $Y_2C_2@C_{3v}$-C_{82} with positive ionization. $Sc_3N@C_{80}$ (m/z = 1109) is an internal standard calibrator. (e) HPLC chromatogram of $Y_2C_2@C_{84}$. (f) LD-TOF mass spectra of ^{13}C enriched $Y_2C_2@C_{84}$ with positive ionization. The smaller peak is M-24 resulted from the loss of a C_2 unit.

approximately 8−10 mg of $Cr(acac)_2$ was added as a relaxation agent. The ^{13}C NMR spectra were obtained utilizing a Bruker 800 MHz (Hollings Marine Laboratory facility) at 298 K with 4 s delay time between pulses. Because of very limited sample quantity of 0.1−1 mg, each spectrum required 2−5 days scan time for the spectra presented.

Computational Studies. Density functional theory (DFT) computations were performed using the Gaussian 03 program package as described in the SI. Briefly, all of the molecules were geometry optimized at the UB3LYP level with a DZVP basis set for yttrium atoms and a 6-31G* basis set for carbon and nitrogen atoms. The energy-minimized values and the same level of theory were used to calculate all of the ^{13}C NMR chemical shifts.[31]

RESULTS

^{13}C NMR Studies of $Y_2C_2@D_3(85)$-C_{92}, $Y_2C_2@C_{3v}$-C_{82}, $Y_2C_2@C_s$-C_{82}, and $Y_2C_2@C_{84}$. The 200 MHz ^{13}C NMR spectrum of $Y_2C_2@C_{92}$ (Figure 4a, aromatic region expanded in Supporting Information Figure S5) shows a series of 15 distinct lines between δ = 128 and 152 ppm. There are 1 double intensity, 13 full intensity, and 1 one-third intensity signals, indicating a 15 × 6, 1 × 2 (number of NMR lines × relative intensity) pattern which is consistent with the C_{92} cage with D_3 symmetry of $Y_2C_2@D_3(85)$-C_{92}, an analogue to the previously reported $Gd_2C_2@D_3(85)$-C_{92} structure.[22] The DFT computational ^{13}C NMR chemical shift range, 129.47−153.15 ppm, is also in good agreement with the range of the experimental spectrum, 128.97−151.69 ppm. One deshielded triplet signal was detected at a chemical shift of δ = 227.3 ppm which originates from the carbide in $Y_2C_2@D_3(85)$-C_{92}. Of special interest is the observed sharp triplet (1:2:1 pattern) signals which is consistent with an yttrium−carbide scalar coupling ($^1J_{YC}$ = 22.4 Hz) between a carbide atom and two chemically equivalent yttrium atoms. To our best knowledge, this is the first observation of a resolved scalar coupling between encapsulated cluster atoms within an EMF cage. The ^{13}C

NMR spectrum of $Y_2C_2@C_{3v}$-C_{82} exhibits 17 signals in the aromatic region (Figure 4c, expanded in Supporting Information Figure S6) and also one highly deshielded signal. The 17 lines consist of 11 full intensity lines (6 carbons), 5 half intensity lines (3 carbons), and 1 one-sixth intensity line (1 carbon), confirming the C_{3v} symmetry of the cage.[18] With ^{13}C isotopic labeling, the ^{13}C NMR deshielded triplet signal was observed at a chemical shift of δ = 257.0 ppm confirming that this signal originates from the carbide in $Y_2C_2@C_{3v}$-C_{82}. This shift is only slightly more deshielded than those reported for $Sc_2C_2@C_{3v}$-C_{82} (δ = 253.2 ppm) and $Sc_2C_2@D_{2d}$-C_{84} (δ = 249.0 ppm) with similar fullerene cages.[23] In similar fashion to $Y_2C_2@D_3$-C_{92}, a sharp triplet (1:2:1 pattern) signal is observed. Of particular interest, the J_{Y-C} coupling of the cluster in $Y_2C_2@C_{3v}$-C_{82} is 17.2 Hz, which is reduced from the 22.4 Hz of $Y_2C_2@C_{3v}$-C_{92}, suggesting a more compressed cluster conformation of the former yttrium carbide EMF in a smaller cage. The ^{13}C NMR spectrum of $Y_2C_2@C_s$-C_{82} shows 44 lines in the aromatic region (expanded as Supporting Information Figure S7), which confirms the identity of the molecule in comparison with previously reported results,[18] and one deshielded signal with a chemical shift of 256.2 ppm. The carbide signal shows the same 1:2:1 pattern resulting from the coupling between ^{89}Y and ^{13}C of the cluster (Figure 4f), with J_{Y-C} coupling of 17.0 Hz. It is important to note that despite the major differences between the cage symmetry of the C_s-C_{82} and C_{3v}-C_{82} cages, the carbide signals from the $(Y_2C_2)^{4+}$ clusters have almost identical chemical shifts and J_{Y-C} coupling constants (Figure 4d,f). This suggests a very similar electronic environment of the $(Y_2C_2)^{4+}$ cluster in these C_{82} cages with very different symmetries. The ^{13}C NMR spectrum of $Y_2C_2@C_{84}$ also shows a highly deshielded carbide signal with the coupling between ^{89}Y and ^{13}C resulting in a 1:2:1 pattern (Figure 4h). The chemical shift
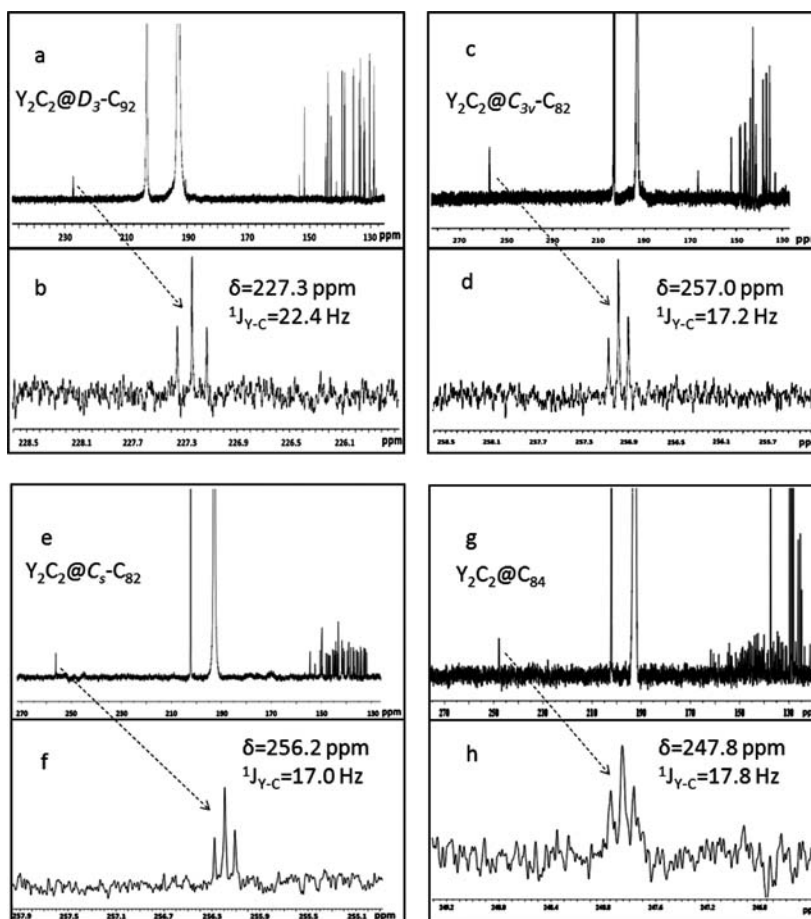
Figure 4. (a) The 200 MHz ^{13}C NMR spectrum of $Y_2C_2@D_3$-C_{92}; (b) expanded region of panel a from 225.8 to 228.6 ppm showing the signal from the endohedral cluster; (c) 200 MHz ^{13}C NMR spectrum of $Y_2C_2@C_{3v}$-C_{82}; (d) expanded region of panel c from 255.4 to 258.6 ppm showing the signal from the endohedral cluster; (e) 200 MHz ^{13}C NMR spectrum of $Y_2C_2@C_s$-C_{82}; (f) expanded region of panle e from 255.1 to 257.9 ppm showing the signal from the endohedral cluster; (g) 200 MHz ^{13}C NMR spectrum of $Y_2C_2@C_{84}$. The tall peaks in the aromatic region are the result of residual solvents (toluene and *o*-xylene). (h) Expanded region of panel g from 246.4 to 249.2 ppm showing the signal from the endohedral cluster.

of this signal is 247.8 ppm, which is slightly more shielded than the signals in both $Y_2C_2@C_{82}$ isomers (256−257 ppm) and much more deshielded than the carbide signal in $Y_2C_2@C_{92}$ (227.3 ppm). In addition, the triplet 1:2:1 pattern is significantly broader in this case and could even possibly suggest a slight inequivalence of the two Y atoms. The J_{Y-C} coupling of the signal is estimated at ~17.8 Hz, which is higher than those of both $Y_2C_2@C_{82}$ isomers but lower than that of the $Y_2C_2@C_{92}$. The poor signal-to-noise ratio in the aromatic region makes it difficult to assign the symmetry of this C_{84} cage. However, we can estimate at least ~70 separate spectral lines in the aromatic region (expanded as Supporting Information Figure S8). In addition, other lines could overlap the toluene solvent impurities in this spectrum. Moreover, the two relatively deshielded peaks at 161.7 and 160.6 ppm are characteristic of fused pentalene carbons,[31] suggesting this C_{84} cage is most likely an isolated pentagon rule (IPR)-violating cage. Future additional studies will be necessary to identify the actual symmetry of this C_{84} cage.

Computational Studies of the $(Y_2C_2)^{4+}$ Cluster. As indicated above, DFT computational studies for the neutral Y_2C_2 molecular cluster support a stable linear structure as illustrated (upper Figure 1a).[28] However, encapsulation of the yttrium carbide cluster involves a charged cluster with transfer of electrons to the fullerene cage. For the charged $(Y_2C_2)^{4+}$

cluster, DFT results also predict a linear structure stable when not encapsulated in a fullerene cage. The DFT computational results predict a carbide ^{13}C NMR chemical shift of 150 ppm and a scalar coupling of $^1J_{YC} = 55.5$ Hz. These values compare favorably with the experimental values reported for the organometallic compound $(Cp)_2YC\equiv CPh\cdot OEt_2$ (147 ppm and 70.9 Hz) and other similar systems where the yttrium atom is also collinear with the carbide moiety ($YC\equiv C$).[32]

DFT Computational Studies of $Y_2C_2@D_5$ (450)-C_{100}, $Y_2C_2@D_3$(85)-C_{92}, and $Y_2C_2@C_{3v}$(8)-C_{82}. On the basis of the optimized geometry of the $(Y_2C_2)^{4+}$, large cages should lead to linear clusters as found above for simpler yttrium carbides. To test this hypothesis, we carried out DFT computations on $(Y_2C_2)^{4+}$ cluster encapsulated in a $D_5(450)$-C_{100} cage ($Y_2C_2@D_5(450)$-C_{100}). The $D_5(450)$-C_{100} cage can be viewed as an icosahedral C_{80} cage cut in half and a nanotube segment (hexagonal carbons) consisting of 20 carbons added in the middle and it was chosen due to its good stability found in other fullerene and metallofullerene studies.[27] The DFT computational study leads to the optimized stable structure illustrated in Figure 5a. The Y atoms in this structure are not exactly linear with the carbide C_2 vector, but are only slightly displaced from the predicted linear $YC\equiv CY$ structure (Y−C−C angle is 22°). In addition, the computed carbide ^{13}C NMR chemical shift of 142.0 ppm and the scalar coupling of $^1J_{YC} =$
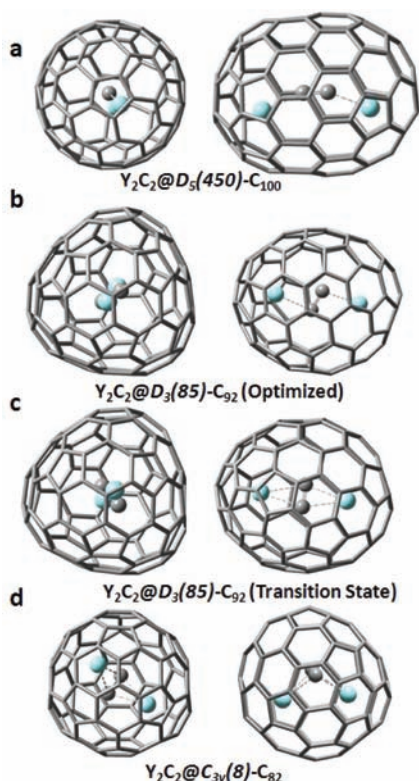
Figure 5. simulated structure of (a) optimized $Y_2C_2@D_5(8)$-C_{100}; (b) optimized $Y_2C_2@D_3(85)$-C_{92}; (c) transition state of $Y_2C_2@D_3(85)$-C_{92}; (d) optimized $Y_2C_2@C_{3v}(450)$-C_{100}.

Figure 6. Cluster motion study with DFT computation. (a) Relative energy of different states of the molecule with rotating $(Y_2C_2)^{4+}$ cluster. The energy values are referenced to the most stable structure. (b) Computed total electron density map of $Y_2C_2@D_3(85)$-C_{92} defining a belt motif with a repulsive interaction between the 5,6,6 junction sites on the cage (blue) and the encapsulated carbide.

57.1 Hz are in good agreement with the prediction for the linear $(Y_2C_2)^{4+}$ cluster (vide supra). Although Y_2C_2 clusters have not been experimentally studied in cages greater that C_{92}, the current computational study predicts linear Y_2C_2 cluster structures are feasible if the fullerene cage is a relatively large cage of at least 100 carbons or has an unusual shape.

The DFT calculations for $Y_2C_2@D_3(85)$-C_{92} suggest an optimized stable structure where the two yttrium atoms are slightly displaced from the C_3 symmetry axis and the carbide vector is nearly orthogonal, but with inequivalent distances of each carbide atom to each yttrium atom (Figure 5b). The transition state (TS) structure of $Y_2C_2@D_3(85)$-C_{92} exhibits an "idealized butterfly shape", where the C_2 carbide unit is perpendicular to a line between the two metal atoms (Figure 5c). The energy difference between the most stable structure and this butterfly structure is only ~12 kJ/mol, which is consistent with the observed ^{13}C NMR sharp triplet (1:2:1 pattern) for a small $(Y_2C_2)^{4+}$ cluster rotational barrier between these two states suggesting rapid motional averaging on the NMR time scale of the carbide atoms about the overall C_3 axis (Figures 5b and 6a). However, the total electron surface map (Figure 6b) defines a belt motif reflecting a significant repulsive interaction with the rotational carbide $(C_2)^{-2}$ at the 3-fold symmetry 6,6,5 junction site of the two pentagons in this belt motif. This suggests rapid carousel rotational motion of the encapsulated C_2 carbide unit about the overall C_3 axis of the $Y_2C_2@D_3(85)$-C_{92} molecule at ambient temperatures.

In the optimized structure of $Y_2C_2@C_{3v}(8)$-C_{82} (Figure 5d), with two yttrium atoms lying along the C_3 axis, the carbide bond is orthogonal to and considerably displaced from the C_3 axi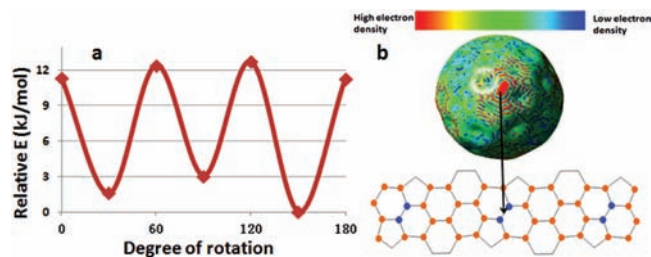s to form a "butterfly", or bent geometry which is suggested by independent computational study of $M_2C_2@C_{3v}(8)$-C_{82} system[33] and experimental study of $Y_2C_2@C_{3v}(8)$-C_{82}.[34]

■ SUMMARY AND DISCUSSION

The experimental and computational results are summarized in Figure 7. It is clear that the $(Y_2C_2)^{4+}$ cluster prefers a linear configuration in the absence of a fullerene cage. However, even in relatively large cages like C_{100}, the cluster adopts a cage only slightly distorted from a linear configuration. For an intermediate cage size, $Y_2C_2@D_3$-C_{92}, the cluster is compressed to make the carbide bond nearly orthogonal to the yttrium bond vector and with only a slightly less stable transition state having an "idealized butterfly" shaped cluster. For a small cage as in the $Y_2C_2@C_{3v}$-C_{82} system, even greater compression is present and the $(Y_2C_2)^{4+}$ cluster adopts a definitive butterfly shape.

It is also clear that the ^{13}C NMR chemical shift and scalar $^1J_{YC}$ coupling parameters provide a very sensitive probe of the degree of NF compression of $(Y_2C_2)^{4+}$ cluster, as illustrated in the right two columns in Figure 7. The ^{13}C NMR results for the carbide signal exhibits a significant deshielding, which increases even more upon NF compression, as the chemical shift increases by over 100 ppm from about 150 ppm for the stretched (nearly linear) clusters (no cage or in D_5-C_{100}) to over 250 ppm for the compressed clusters (C_{3v}-C_{82} and C_s-C_{82}). At the same time, the scalar $^1J_{YC}$ decreases upon NF compression from over 50 Hz for the nearly linear clusters to about 17 Hz found in the compressed clusters in smaller cages (C_{3v}-C_{82} and C_s-C_{82}).

In addition, it is interesting to note that the cage symmetry does not play a decisive role in determining the shape of the cluster structure. For example, $Y_2C_2@C_{3v}$-C_{82} represents a high-symmetry case with only 17 NMR signals for 82 aromatic carbon atoms, while $Y_2C_2@C_s$-C_{82} represents the low-symmetry case with 44 NMR signals for the 82 aromatic carbon atoms. Despite these major differences in cage symmetry (C_{3v} versus C_s), they have very similar chemical shifts (257.0 ppm vs 256.2 ppm) and $^1J_{YC}$ couplings (17.2 ppm vs 17.0 ppm) for the yttrium carbide clusters. Also, the $Y_2C_2@C_{84}$ shows a carbide signal with 247.8 ppm chemical shift and $^1J_{YC}$ = 18.0 Hz which both agree with the NF compression trend very well, indicating the unique pentalene motif only has a limited influence on the cluster structure and NMR parameters. These results suggest that cage symmetry for a given cage size (C_{82}) plays only a minor role in influencing the ^{13}C NMR spectral parameters and corresponding shape of the $(Y_2C_2)^{4+}$ cluster. In summary, the more important factor in dictating the structure of the

Molecule	Optimized cluster structure	Average atomic distance in the cluster Y-C/Y-Y/C-C (Å)	C_2 ^{13}C NMR chemical shift (ppm)	$^1J_{Y-C}$ (Hz)
$(Y_2C_2)^{4+}$		2.92/5.83/1.27	147* (150)	70.9* (55.5)
$Y_2C_2@D_5\text{-}C_{100}$		2.89/5.51/1.26	(156)	(57.1)
$Y_2C_2@D_3\text{-}C_{92}$ (opt)		2.53/4.92/1.27	227.3 (229)	22.4 (22.5**)
$Y_2C_2@D_3\text{-}C_{92}$ (TS)		2.48/4.81/1.27	(288)	(21.6)
$Y_2C_2@C_{84}$	--	--	247.8	17.8
$Y_2C_2@C_{3v}\text{-}C_{82}$		2.43/3.74/1.27	257.0 (288)	17.2 (18.3)
$Y_2C_2@C_s\text{-}C_{82}$	--	--	256.2	17.0

Numbers in parentheses are computational results.

* These values represent the experimental result of $(Cp)_2YC\equiv CPh\bullet OEt_2$
**This number represents average value of the scalar coupling constants between Y atom and carbon 1 (40.6 Hz) and carbon 2 (4.4 Hz)

Figure 7. Key results from NMR experiments and DFT calculations.

encapsulated $(Y_2C_2)^{4+}$ cluster is the carbon cage size. However, it is possible that for significantly larger EMFs the cage structure may play a more important role.

Also summarized in Figure 7, the atomic distances within the $(Y_2C_2)^{4+}$ cluster provided by DFT computation suggests that the cluster atoms are forced closer with increasing compression, as indicated by the decrease of both Y−C distance (average of Y−C1 and Y−C2) and Y−Y distance. It should be noted that the C−C distance remains almost unchanged within the bond length uncertainty limits. It is also interesting to note that the alteration in cluster atomic distances under NF compression exhibits the same trend as the lattice atomic distances for the yttrium carbide Y_2C_3 system under compression by macroscopic pressure (MP),[3] as shown in Figure 8. In both systems, the Y−C and Y−Y distances decrease with increasing compression, either from smaller fullerene cage or a higher external pressure. Moreover, the C−C distances remain nearly constant in both cases. Qualitatively, decreasing cage size by ~18 carbons within the investigated region (~C_{82}−C_{100}) in NF compression is nearly equivalent to increasing the external pressure from 0 to 50 GPa in MP compression based on the changes in Y−C interatomic distance. The Y−C distance under the upper limit of pressure ~50 GPa is also reflective of the experimental limit to date for the smallest cages (~C_{80}, see Figure 1e) that can potentially be isolated. It is worth mentioning that such contraction upon MP compression is not limited to the yttrium carbide (Y_2C_3), but has also been studies in lanthanum carbide systems as well.[35]

■ CONCLUSION

In this paper, we have synthesized, purified, and characterized from a diyttrium metallofullerene family, four yttrium carbide endohedral metallofullerenes (EMFs), $Y_2C_2@D_3(85)\text{-}C_{92}$, $Y_2C_2@C_{3v}\text{-}C_{82}$, $Y_2C_2@C_s\text{-}C_{82}$, and $Y_2C_2@C_{84}$. We have investigated the $(Y_2C_2)^{4+}$ cluster structural features in this EMF family by ^{13}C NMR and DFT computational approaches. With the chemical shift and first-time observation of metal-carbide $^1J_{YC}$ coupling of the $(Y_2C_2)^{4+}$ cluster, we have probed the structural change of the endohedral clusters under the
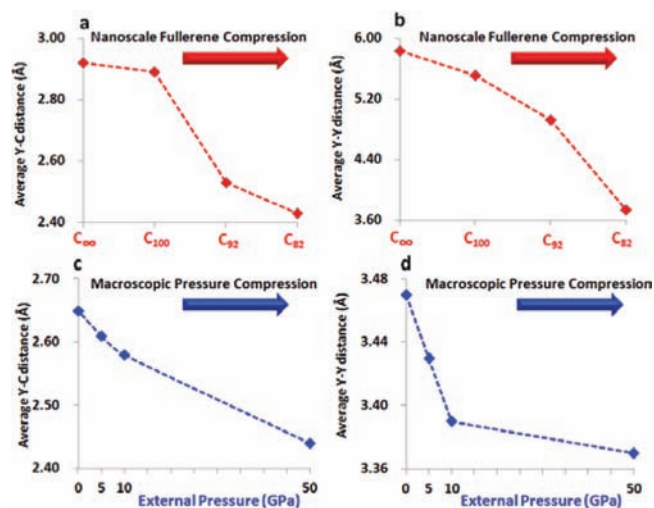

Figure 8. The change of interatomic distances upon on compression. Red lines and points denote the data obtained from NFC (data source Figure 7, C_∞ represents the calculated interatomic distances for $[Y_2C_2]^{4+}$ cluster), and blue lines and points denote the data obtained from MPC (data source ref 3 and transferred as in Figure S13 in Supporting Information). Y−C distances are average values of corresponding Y−C1, Y−C2, and Y−C3 distance in the lattice. Y−Y distances are average values of corresponding Y−Y1 and Y−Y2 distance in the lattice). (a) Y−C distances in fullerene cages; (b) Y−Y distances in fullerene cages; (c) Y−C distances in superconducting materials; (d) Y−Y distances in superconducting materials.

influence of NF compression. The ^{13}C NMR chemical shift and scalar $^1J_{YC}$ coupling parameters provide a very sensitive measure of the structural changes of the $(Y_2C_2)^{4+}$ cluster with respect to changes in the size of the carbon cage (C_{82}−C_{100}). In contrast with changes in the size of the cage, the results suggest only a minor role for changes in cage symmetry for a given cage size (C_{82}) as reflected by influences on the ^{13}C NMR spectral parameters. These results confirm the hypothesis that influence of nanoscale fullerene compression (NFC) on interatomic distances on yttrium carbide clusters is consistent with the influence of macroscopic pressure compression (MPC). With

the support of DFT calculation results, one can conclude that upon NFC the cluster changed from a stretched linear shape to a compressed "butterfly shape", with increasing chemical shift values, decreasing $^1J_{Y-C}$ coupling constants and decreasing Y−C interatomic distances found for the clusters. The crystal structural parameters of a previously reported metal carbide Y_2C_3 are directly compared to the $(Y_2C_2)^{4+}$ cluster in the current metallofullerene study illustrating the influence of nanoscale FC when compared with the effects of macroscopic PC. In the future, the possibility of using EMFs as isolated ideal model clusters to mimic other metal lattice clusters under ultrahigh pressure could be important in metal carbide materials research.

■ ASSOCIATED CONTENT

Ⓢ Supporting Information

Detailed computational methods, UV−vis spectra of the four isolated yttrium carbide EMFs, expanded aromatic region of the 4 NMR spectra, simulated ^{13}C NMR aromatic regions, cyclic voltammetry of $Y_2C_2@D_3$-C_{92}, interatomic distance table in Y_2C_3 lattice from ref 3, coordinates of optimized structures and TS structures. This material is available free of charge via the Internet at http://pubs.acs.org.

■ AUTHOR INFORMATION

Corresponding Author

hdorn@vt.edu

Notes

The authors declare no competing financial interest.

■ ACKNOWLEDGMENTS

■ REFERENCES

(1) Kurotobi, K.; Murata, Y. Science 2011, 333, 613.

(2) Nakane, T.; Naka, T.; Kito, H.; Wada, T.; Matsushita, A.; Kumakura, H.; Mochiku, T. Physica C 2005, 426, 492.

(3) Yu, C.; Liu, J. Y.; Lu, H.; Li, P. L.; Fan, R. Z.; Xiao, J. Y. Solid State Commun. 2007, 142, 536.

(4) Amano, G.; Akutagawa, S.; Muranaka, T.; Zenitani, Y.; Akimitsu, J. J. Phys. Soc. Jpn. 2004, 73, 530.

(5) Chai, Y.; Guo, T.; Jin, C. M.; Haufler, R. E.; Chibante, L. P. F; Fure, J.; Wang, L. H.; Alford, J. M.; Smalley, R. E. J. Phys. Chem. 1991, 95, 7564.

(6) Shinohara, H.; Sato, H.; Saito, Y.; Ohkohchi, M.; Ando, Y. J. Phys. Chem. 1992, 96, 3571.

(7) Wakahara, T.; Okubo, S.; Kondo, M.; Maeda, Y.; Akasaka, T.; Waelchli, M.; Kako, M.; Kobayashi, K.; Nagase, S.; Kato, T.; Yamamoto, K.; Gao, X.; Van Caemelbecke, E.; Kadish, K. M. Chem. Phys. Lett. 2002, 360, 235.

(8) Wakahara, T.; Kobayashi, J.; Yamada, M.; Maeda, Y.; Tsuchiya, T.; Okamura, M.; Akasaka, T.; Waelchli, M.; Kobayashi, K.; Nagase, S.; Kato, T.; Kako, M.; Yamamoto, K.; Kadish, K. M. J. Am. Chem. Soc. 2004, 126, 4883.

(9) Akasaka, T.; Kono, T.; Takematsu, Y.; Nikawa, H.; Nakahodo, T.; Wakahara, T.; Ishitsuka, M. O.; Tsuchiya, T.; Maeda, Y.; Liu, M. T. H.; Yoza, K.; Kato, T.; Yamamoto, K.; Mizorogi, N.; Slanina, Z.; Nagase, S. J. Am. Chem. Soc. 2008, 130, 12840.

(10) Wang, C. R.; Kai, T.; Tomiyama, T.; Yoshida, T.; Kobayashi, Y.; Nishibori, E.; Takata, M.; Sakata, M.; Shinohara, H. Nature 2000, 408, 426.

(11) Kato, H.; Taninaka, A.; Sugai, T.; Shinohara, H. J. Am. Chem. Soc. 2003, 125, 7782.

(12) Lu, X.; Nikawa, H.; Nakahodo, T.; Tsuchiya, T.; Ishitsuka, M. O.; Maeda, Y.; Akasaka, T.; Toki, M.; Sawa, H.; Slanina, Z.; Mizorogi, N.; Nagase, S. J. Am. Chem. Soc. 2008, 130, 9129.

(13) Cao, B.; Nikawa, H.; Nakahodo, T.; Tsuchiya, T.; Maeda, Y.; Akasaka, T.; Sawa, H.; Slanina, Z.; Mizorogi, N.; Nagase, S. J. Am. Chem. Soc. 2008, 130, 983.

(14) Yamada, M.; Wakahara, T.; Tsuchiya, T.; Maeda, Y.; Akasaka, T.; Mizorogi, N.; Nagase, S. J. Phys. Chem. A 2008, 112, 7627.

(15) Stevenson, S.; Rice, G.; Glass, T.; Harich, K.; Cromer, F.; Jordan, M. R.; Craft, J.; Hadju, E.; Bible, R.; Olmstead, M. M.; Maitra, K.; Fisher, A. J.; Balch, A. L.; Dorn, H. C. Nature 1999, 401, 55.

(16) Dunsch, L.; Yang, S. Small 2007, 3, 1298.

(17) Wang, C. R.; Kai, T.; Tomiyama, T.; Yoshida, T.; Kobayashi, Y.; Nishibori, E.; Takata, M.; Sakata, M.; Shinohara, H. Angew. Chem., Int. Ed. 2001, 40, 397.

(18) Inoue, T.; Tomiyama, T.; Sugai, T.; Okazaki, T.; Suematsu, T.; Fujii, N.; Utsumi, H.; Nojima, K.; Shinohara, H. J. Phys. Chem. B 2004, 108, 7573.

(19) Tan, K.; Lu, X. Chem. Commun. 2005, 4444.

(20) Liduka, Y.; Wakahara, T.; Nakahodo, T.; Tsuchiya, T.; Sakuraba, A.; Maeda, Y.; Akasaka, T.; Yoza, K.; Horn, E.; Kato, T.; Liu, M. T. H.; Mizorogi, N.; Kobayashi, K.; Nagase, S. J. Am. Chem. Soc. 2005, 127, 12500.

(21) Shi, Z. Q.; Wu, X.; Wang, C. R.; Lu, X.; Shinohara, H. Angew. Chem., Int. Ed. 2006, 45, 2107.

(22) Yang, H.; Lu, C.; Liu, Z.; Jin, H.; Che, Y.; Olmstead, M. M.; Balch, A. L. J. Am. Chem. Soc. 2008, 130, 17296.

(23) Yamazaki, Y.; Nakajima, K.; Wakahara, T.; Tsuchiya, T.; Ishitsuka, M. O.; Maeda, Y.; Akasaka, T.; Waelchli, M.; Mizorogi, N.; Nagase, S. Angew. Chem., Int. Ed. 2008, 47, 7905.

(24) Kurihara, H.; Lu, X.; Iiduka, Y.; Mizorogi, N.; Slanina, Z.; Tsuchiya, T.; Akasaka, T.; Nagase, S. J. Am. Chem. Soc. 2011, 133, 2382.

(25) Kurihara, H.; Lu, X.; Iiduka, Y.; Nikawa, H.; Hachiya, M.; Mizorogi, N.; Slanina, Z.; Tsuchiya, T.; Nagase, S.; Akasaka, T. Inorg. Chem. 2011, 51, 746.

(26) Iiduka, Y.; Wakahara, T.; Nakajima, K.; Nakahodo, T.; Tsuchiya, T.; Maeda, Y.; Akasaka, T.; Yoza, K.; Liu, M. T. H.; Mizorogi, N.; Nagase, S. Angew. Chem., Int. Ed. 2007, 46, 5562.

(27) Yang, T.; Zhao, X.; Nagase, S. Phys. Chem. Chem. Phys. 2011, 13, 5034.

(28) Roszak, S.; Balasubramanian, K. J. Phys. Chem. A 1998, 102, 6004.

(29) Stevenson, S.; Harich, K.; Yu, H.; Stephen, R. R.; Heaps, D.; Coumbe, C.; Phillips, J. P. J. Am. Chem. Soc. 2006, 128, 8829.

(30) Burke, B. G.; Chan, J.; Williams, K. A.; Fuhrer, T.; Fu, W.; Dorn, H. C.; Puretzky, A. A.; Geohegan, D. B. Phys. Rev. B 2011, 83, 115457.

(31) Fu, W.; Xu, L.; Azurmendi, H.; Ge, J.; Fuhrer, T.; Zuo, T.; Reid, J.; Shu, C.; Harich, K.; Dorn, H. C. J. Am. Chem. Soc. 2009, 131, 11762.

(32) Denhaan, K. H.; Wielstra, Y.; Teuben, J. H. Organometallics 1987, 6, 2053.

(33) Valencia, R.; Rodriguez-Fortea, A.; Poblet, J. M. J. Phys. Chem. A 2008, 112, 4550.

(34) Nishibori, E.; Ishihara, M.; Takata, M.; Sakata, M.; Ito, Y.; Inoue, T.; Shinohara, H. Chem. Phys. Lett. 2006, 433, 120.

(35) Wang, X.; Loa, I.; Syassen, K.; Kremer, R. K.; Simon, A.; Hanfland, M.; Ahn, K. Phys. Rev. B 2005, 72, No. 064520.

8493

dx.doi.org/10.1021/ja300134x | J. Am. Chem. Soc. 2012, 134, 8487−8493